Applied Surface Science 505 (2020) 144650

Contents lists available at ScienceDirect

Applied Surface Science

journal homepage: www.elsevier.com/locate/apsusc

Full Length Article

Impact of the interface vacancy on Schottky barrier height for Au/AlN polar interfaces

Hailing Guo[a,1], Zhaofu Zhang[b,1,*], Yuzheng Guo[c], Zhibin Gao[d], Ruisheng Zheng[a], Honglei Wu[a,*]

[a] College of Physics and Optoelectronic Engineering, Shenzhen University, Shenzhen 518060, China
[b] Department of Engineering, University of Cambridge, Cambridge CB2 1PZ, United Kingdom
[c] College of Engineering, Swansea University, Swansea SA1 8EN, United Kingdom
[d] Department of Physics, National University of Singapore, Singapore 117551, Republic of Singapore

ARTICLE INFO

Keywords:
AlN polar surface
Schottky barrier heights
Interface vacancy
First-principles calculation

ABSTRACT

Schottky barrier heights (SBHs) at the Au/AlN interface are systemically studied by density functional calculations. Two types of interfaces, including Al- and N-polar interfaces, are constructed to examine the relationship between the SBH and the interfacial atom species. An in-depth exploration is conducted by introducing interfacial aluminum vacancy or nitride vacancy. The results show that the calculated *p*-type SBH of the Al-polar interface (2.30 eV) is higher than that of the N-polar interface (1.23 eV). Results also show that the SBH of the interface with Al or N vacancies would be higher. More obvious metal-induced gap states (MIGS) can be observed after the introduction of interfacial vacancy site, leading to a stronger Fermi-level pinning at the contact. The derived SBHs are within the reported measurement range. The findings provide an insightful hint for AlN-based devices where Schottky contact matters.

1. Introduction

Wurtzite aluminum nitride (AlN) has attracted extensive attention for optical and electronic applications [1,2]. AlN holds promise for high-temperature applications and high-power devices due to its high thermal conductivity, high critical electric field and wide bandgap energy applications [3–6]. Many methods have been exploited to realize the heteroepitaxial growth of AlN, including hydride vapor phase epitaxy (HVPE), metal-organic chemical vapor deposition (MOCVD), molecular beam epitaxy (MBE), and physical vapor technique (PVT) [7–10]. To date, bulk AlN single crystals of large size and high quality have become available, leading to the rapid development of AlN-based devices [11,12]. Besides, researches have shown doping AlN with nonmagnetic transition metals is a novel way for designing new-functional devices [13,14]. Therefore, based on the achievements on AlN crystal, a thorough understanding on the electronic structures of AlN-based devices is highly desirable.

SBH is one of the most momentous parameters determining the transport properties and an important factor for fabricating electronic devices [15]. An extremely low (or even negative) SBH value is desirable for a linear current-voltage relationship, namely transparent, ohmic contact [16], while a high SBH is a prerequisite for a Schottky contact. Schottky contact rather than ohmic case is normally formed at the interface between AlN and metals and a series of studies have been conducted to better understand the transport properties [17–19]. Reddy *et al.* [17] have investigated the band alignment by internal photoemission and demonstrated the *p*-type Schottky contact between AlN and Au. Slepko *et al.* [18] focused on theoretical investigations on SBHs with different metals. Despite the progress in the fabrication of Au/AlN heterojunctions, a deeper understanding of their electronic structures is still lacking, and some fundamental issues still need to be solved. Especially, during the crystal growth, semiconductor defects, such as vacancies, would be easily induced and the influence of these defects on the SBH has not been explored. Therefore, a comprehensive understanding of the heterostructures is desirable for the future development of AlN-based devices.

In this work, the SBH's dependence on interface atomic structure for Au/AlN polar interfaces is investigated. The pristine interface structures including the Al- and N- polar cases are examined. Besides, defective interfaces including aluminum (V_{Al}) and nitrogen vacancies at the interface (V_N) are considered to carry out an in-depth study. Results demonstrate that the interfacial structures have a significant effect on the electronic properties of Au/AlN polar interfaces.

* Corresponding authors.
E-mail addresses: zz389@cam.ac.uk (Z. Zhang), hlwu@szu.edu.cn (H. Wu).
[1] The authors contribute equally to this work.

https://doi.org/10.1016/j.apsusc.2019.144650
Received 29 August 2019; Received in revised form 24 October 2019; Accepted 8 November 2019
Available online 15 November 2019
0169-4332/ © 2019 Elsevier B.V. All rights reserved.

2. Calculation details

All calculations were carried out with the plane-wave CASTEP code based on density function theory (DTF) [20]. The norm-conserving pseudopotential was employed to describe the electron-ion interaction. An energy cutoff of 700 eV and a k-mesh grid of 4 × 4 × 1 were used. Perdew-Burke-Ernzerbof (PBE) version of GGA was utilized to optimize the atomic structures [21]. The convergence threshold for maximum forces on the atoms was 0.03 eV/ Å. The optimized geometric structures were calculated by Heyd-Scuseria-Ernzerh of (HSE) hybrid function due to the bandgap narrowing caused by the semi-local exchange-correction functional [22]. The Hartree-Fock exchange fraction was tested to be 33%, producing the direct band-gap of 6.1 eV for AlN, in good agreement with the experimental band gap value [23,24].

The AlN hexagonal structure along the c-axis is characterized by bilayer configurations on the basal plane and the polarity of AlN can be determined by the topmost atom species. For the Al-polar (0001) surface, Al atoms occupy the top position of the bilayer, while N atoms occupy the top position for the N-polar (000$\bar{1}$) surface. The AlN crystal with different polar surface possesses different structural and electronic properties and this have been verified experimentally and theoretically [25,26]. In this work, two AlN polar surfaces, both the N-polar and Al-polar surfaces, were utilized to construct the heterostructures on which the Au slab is placed. The lattice constants of AlN were fixed to its optimized values, and the overall strain induced in Au was 5.3%, which would not induce significant changes in its electronic structure [27,28]. Specifically, AlN slab with (2 × 2) in-plane periodicity and six bilayers was brought into contact with the five-layer Au slab. Additionally, a vacuum thickness of 15 Å was added to avoid the interactions between imaging slabs. The bottom termination of Al or N atoms were passivated with pseudohydrogen. The bottom two-bilayer AlN atoms were frozen in the structural optimization.

To study the impact of interfacial vacancy on the SBH, one of the four interfacial Al (or N) atoms was removed, leading to a 25% interfacial vacancy ratio. To sum up, four types of Au/AlN interfaces are considered in this work: Al-terminated pristine interface (denoted as Al-pristine interface), N-terminated pristine interface (N-pristine interface), Al-terminated interface with an interfacial Al vacancy site (Al-V_{Al} interface) and N-terminated interface with an interfacial N vacancy site (N-V_N interface). In this work, a detailed study is initially carried out to search for the energy-favorable configurations for further analysis, considering DFT cannot accurately and readily locate the global energy minimum. Subsequently, the contacts between AlN and Au with and without defects are systemically evaluated. Finally, the SBH values for different heterostructures are compared.

3. Results and discussions

Several interface configurations with high-symmetry atomic arrangement are tested initially as we did previously [29]. Four possible initial geometries are considered for both pristine Al- and N- terminated interfaces: (a) Au sites above the hollow sites of AlN (denoted as the hollow model), (b) Au lies on the bridge sites of AlN (the bridging model), (c) Au sits on top of the surface atoms of Al or N (the Al-ontop model for Al-face and N-ontop model for N-face), (d) Au locates above the second-layer N atoms or Al atoms (the N-ontop model for Al interface and Al-ontop model for N interface). The schematic structures are displayed in Fig. 1 and the total energy of these models with varied slab distances are depicted in Fig. 2. The structures with the lowest energy are further employed for the optimization.

The most stable interlayer distance and corresponding interface binding energy of the eight configurations after being fully optimized are summarized in Table 1. The binding energy (E_b), which can characterize the intralayer interaction strength, is defined as:

$$E_b = (E_{AlN/Au} - E_{AlN} - E_{Au})/S \quad (1)$$

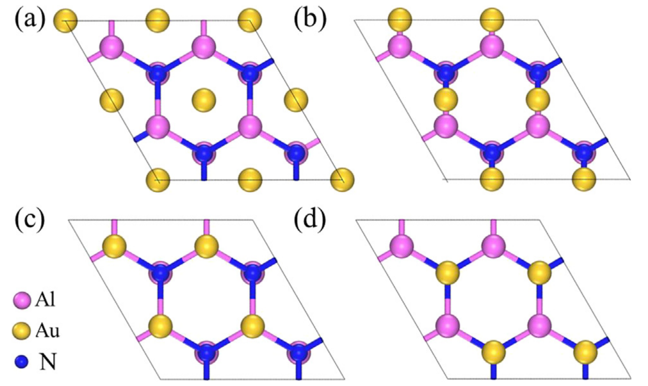

Fig. 1. Top views of the Au/AlN heterostructures with different stacking configurations: (a) the hollow model, (b) the bridging model, (c) Al-ontop model and (d) N-ontop model, respectively. The Al-terminated interface is taken as an example and only the interfacial Au layer atoms are displayed. The purple, yellow and blue spheres denote Al, Au, and N atoms, respectively. (For interpretation of the references to colour in this figure legend, the reader is referred to the web version of this article.)

where $E_{AlN/Au}$, E_{AlN}, and E_{Au} represent the total energy the interface model, isolated AlN slab and Au slab, respectively, and S is the surface area. Notably, the smaller E_b value indicates stronger adhesion between Au and AlN. As depicted in Table 1, for Al-terminated heterostructures, Au atoms preferentially occupy surface hollow sites (i.e., Model a in Fig. 2(a), the hollow model) with the lowest binding energy of -0.20 eV/Å^2, whereas the most stable structure for N-terminated interface is the N-ontop configuration (Model b in Fig. 2(b)) with the binding energy of -0.17 eV/Å^2.

All the structures after being fully relaxed are illustrated in Fig. 3, which apparently undergo interface atomic rearrangement. The adjustments are more pronounced in the Al-V_{Al} interface, namely, Au atom at the interface shows a tendency to fill the vacancy site. The interlayer separation for heterojunctions with V_{Al} and V_N are increased to be 2.29 Å and 2.16 Å, respectively, while that for corresponding pristine models are 2.19 Å and 2.08 Å, indicating a weaker interaction for the defective models.

Vacancies existing in the electronics would affect the electron transport. Hence, a vacancy site was introduced into the pristine system to study its impact on the SBH. The formation energy of the neutral vacancy is defined as [30]:

$$E_f = E_{pristine} - E_{defect} + n\mu_m \quad (2)$$

in which $E_{pristine}$ and E_{defect} are the total energies of the pristine and defective structure, respectively. n and μ_m represent the number and chemical potential of the removed atom, respectively. The results are derived in N-rich condition, which is the typical growth environment for AlN crystal with PVT method [10]. The formation energies of Al vacancy and N vacancy in N-rich limit are 1.98 eV and 3.02 eV, respectively, indicating the stable formation of the Al vacancy and N vacancy site. The results are in good correspondence with the theoretical values reported before [31].

Further insights into the interaction between AlN and Au can be attained from charge difference analysis. The differential charge density Δρ(z) along the perpendicular direction are quantitatively plotted in Fig. 4. The electron density difference is measured by:

$$\Delta\rho(z) = \rho_{interface}(z) - \rho_{Au}(z) - \rho_{AlN}(z) \quad (3)$$

where $\rho_{interface}(z)$, $\rho_{Au}(z)$ and $\rho_{AlN}(z)$ are the plane-averaged electron density of the interface, the metal adsorbate, and semiconductor substrate, respectively. The positive values indicate electron accumulation while the negative values represent depletion. Obviously, the most significant charge transfer oscillations are confined at the interfacial region and that attenuates while moving away from the interface. Due

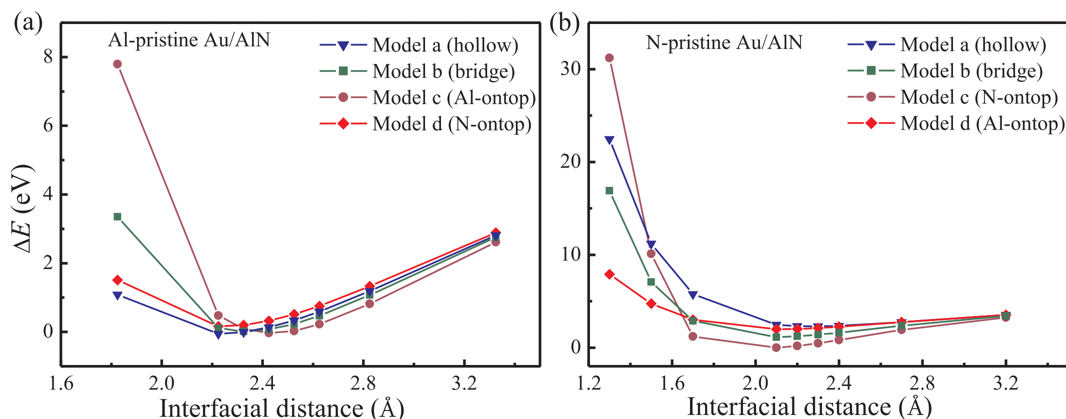

Fig. 2. The relative total energy ΔE of the heterojunctions for (a) Al-terminated interface and (b) N-terminated interface with respect to different interlayer distances. The total energy of the most stable interface configuration is referred as 0 eV.

Table 1
Binding energy E_b (eV/Å^2) and interlayer distance d_0 (Å) for the most stable Al-terminated and N-terminated interfaces with different interfacial configurations.

Interface model	Configuration	E_b (eV/Å^2)	d_0 (Å)
Al-terminated interface	Hollow	−0.20	2.19
	Bridge	−0.19	2.33
	Al-ontop	−0.18	2.47
	N-ontop	−0.19	2.23
N-terminated interface	Hollow	−0.10	2.15
	Bridge	−0.16	2.14
	N-ontop	−0.17	2.08
	Al-ontop	−0.08	2.14

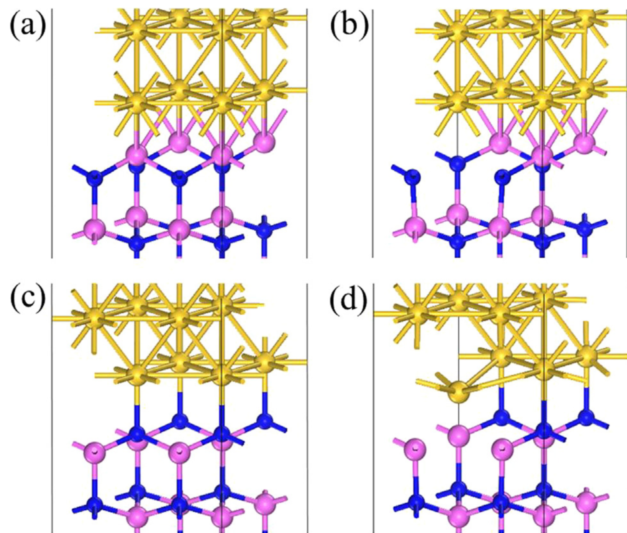

Fig. 3. Structure diagrams of the relaxed supercell heterojunction for (a) Al-pristine, (b) Al-V_{Al}, (c) N-pristine, (d) N-V_N configurations, respectively.

the interfacial dipole caused by the different work function of the two slabs, charge transfer occurs so that the interface contact can share the same Fermi level. Besides, in the case of Al-pristine and Al-V_{Al} systems, charge depletion mainly arises in both the semiconductor and the metal sides. Then an excess of charge is formed at the interface. And for N-pristine and N-V_N systems, the different trends are found, namely, an asymmetric charge accumulation is found across the interface. This tendency is similar to the relation between the Zn-terminated and O-terminated ZnO/Ag interfaces [32].

To further demonstrate the bonding behavior at the interface, the Mulliken bond population analysis was also performed to explore the bond overlap population. It serves as a useful bonding index, and the type of bonding and its value can be determined by calculating the bond population. The ionicity scale based on bond overlap population can be defined as [33]:

$$P_i = 1 - exp[-|P_c - P|\ P] \quad (4)$$

where P is the overlap population for a bond, P_c is the bond population for a purely covalent bond. P_i is equal to zero for a purely covalent bond and to unity for a purely ionic bond. And a high value of bond population implies a covalent bond while a low value indicates an ionic interaction. Table 2 lists the bond length and bond overlap population analysis of the four heterojunctions. The bond population values for N-pristine and N-V_N interface are 0.49 and 0.40, sitting between 0.22 of ionic NaCl and 0.87 of covalent Si [34], revealing the mixing of covalent and ionic bonding with the dominance of covalent nature for the N-pristine and N-V_N interface. Moreover, the bond population for Al-pristine and Al-V_{Al} interface are 0.13 and 0.09, respectively, indicating the dominance of ionic character in the interface. Based on the analyses above, the chemical bonds connecting AlN of different polar surfaces and Au show different features. In addition, the bond lengths of the imperfective structures are larger than that of the pristine models, indicating a weaker interaction, and the results agree with the previous discussion on the binding energy.

Local density-of-states (DOS) projected on the four AlN bilayers and interfacial Au layer are shown in Fig. 5. The PDOS of the interface AlN bilayers apparently reveals the existence of metal-induced gap states (MIGS) [35,36], which occurs within the band gap at the AlN surface layers. These states can be thought of as the evanescent states of the metal wave functions continued into the forbidden energy gap of the semiconductor. When AlN contacts with Au, the travelling wave states of metal Au will not disappear immediately, instead they will propagate into the AlN side. But these states are evanescent and the MIGS decay occurs simultaneously with its propagation into AlN. This method has been widely used by us and other groups [27,28,32]. As shown in the DOS figures, these surface states decrease rapidly, and the bulk conditions are well recovered in the third layer of AlN. Moreover, more gap states within the band gap could be observed in the interface with vacancy (especially the Al-V_{Al} case in Fig. 5(b)), indicating a stronger MIGS effect. Further insights into the nature of the gap states are investigated through their spatial distribution in Fig. 6. The plotted orbital showed in Fig. 6 is the square of the absolute value of the wave-function for the band around Fermi level summed over all the k-points [37]. Obviously, these states show a visible behavior in the interfacial Au region but a negligible dispersion at the AlN side. And a more scattering tendency could be found in the defective interfaces, consistent with the enhancement of Fermi-level pining.

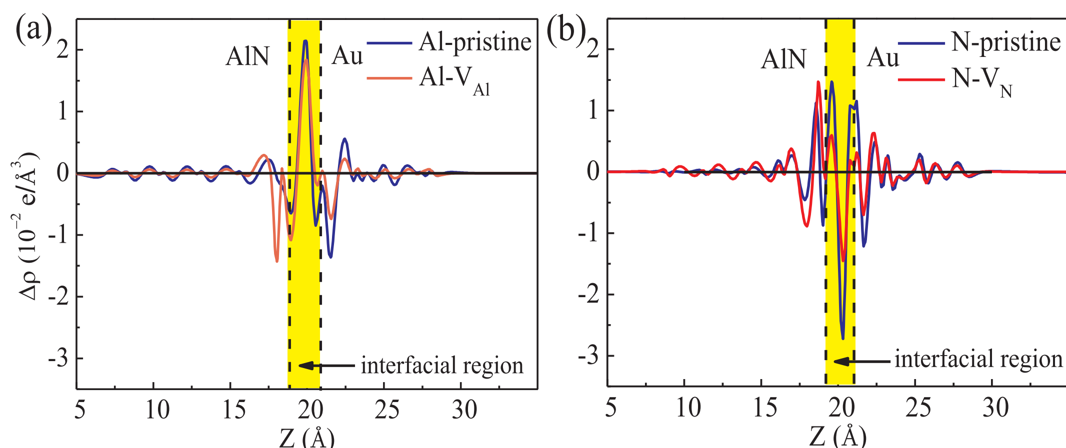

Fig. 4. The differential charge density Δρ (z) along the normal direction for (a) Al-pristine and Al-V_{Al}, (b) N-pristine and N-V_N system.

Table 2
Mulliken bond population analysis between the nearest-neighbor interfacial atoms for the four heterostructures.

System	Bond	Length (Å)	Population
Al-pristine	Au-Al	2.81	0.13
Al-V_{Al}		2.93	0.09
N-pristine	Au-N	2.14	0.49
N-V_N		2.16	0.40

Metal-semiconductor junction is a critical component in electronic and optoelectronic devices. As aforementioned, one of the most important parameters for this junction is the Schottky barrier height. The energy for charge carrier transport across the junction plays a crucial role in device performance [38,39]. Estimation of SBH at the metal-semiconductor interface can be deduced by two limits. According to the Schottky-Mott model, the SBH is defined as the energy difference between the work function of metal and the electron affinity of the semiconductor. However, some evidence have proven the insensitivity of the SBH to metals and this phenomenon can be explained by the Bardeen limit where the SBH is determined by the surface states in the band gap of the semiconductor [35,36]. Besides, previous studies have shown the SBH's reliance on the practical interface structure [40]. For instance, the oxygen vacancies would produce a significant impact on

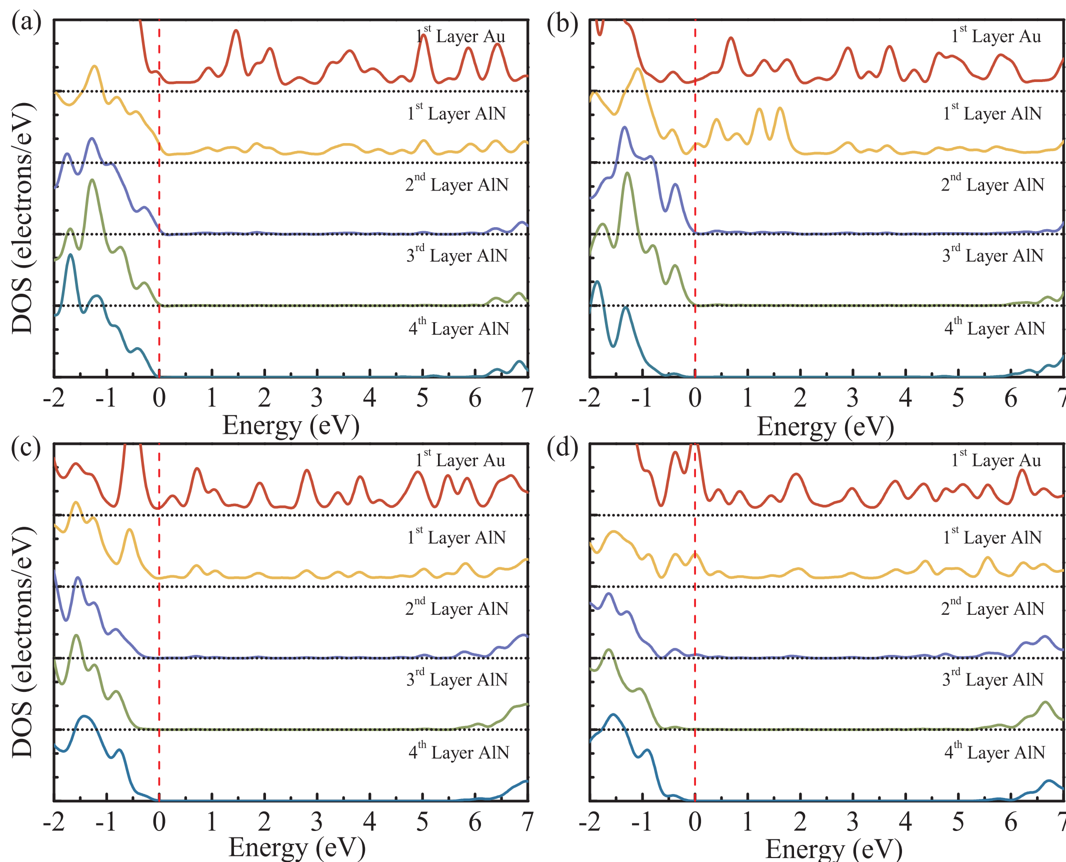

Fig. 5. Layer-resolved DOS of Au and AlN individual layers for (a) Al-pristine, (b) Al-V_{Al}, (c) N-pristine, and (d) N-V_N systems, respectively. The yellow, blue, green, cyan lines indicate the 1st, 2nd, 3rd and 4th AlN atomic bilayer (counting from the interface contact), respectively. The red line indicates the 1st layer of Au. The decay of MIGS can be clearly observed. The Fermi energy is aligned at zero.

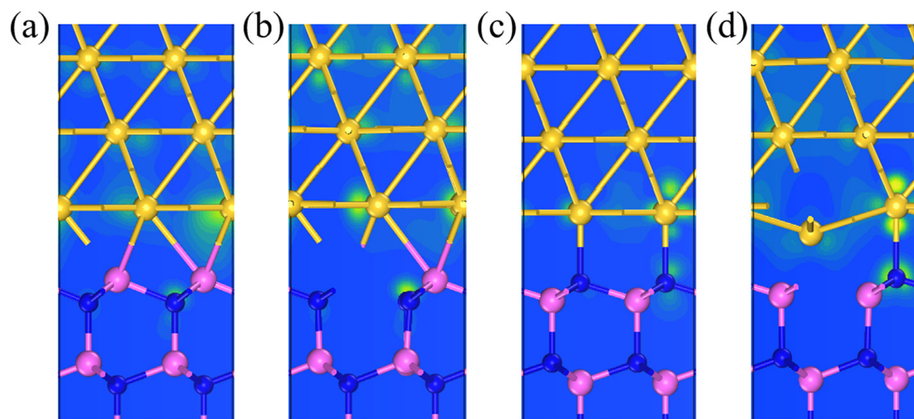

Fig. 6. Wavefunction orbitals around Fermi energy for (a) Al-pristine, (b) Al-V_{Al}, (c) N-pristine, and (d) N-V_N systems, respectively.

Table 3
Comparison between the calculated Schottky barrier height for the heterostructures and that from references.

Heterojunction	This work (eV)	Reference (eV)
Al-pristine	2.30	2.70 [17]
Al-V_{Al}	2.41	–
N-pristine	1.23	2.00 [46]
N-V_N	2.21	–

the SBHs for ZnO-based Schottky contacts [41,42].

Generally, the *p*-type SBH can be defined as the energy difference between the Fermi level of the heterojunction and the valence band edge of the semiconductor. The core-level method is adopted in this work to analyze the SBH values. This approach is accurate on the assumption that in the heterostructure the energy difference of the selected core states with respect to the valence band maximum maintains the same value with that of the bulk structures when the selected atoms are far from the interface [27,28,43]. The derived SBHs are summarized in Table 3, and the experimental SBH results are also listed for comparison.

The obtained *p*-type SBH for the Al-pristine and N-pristine model is 2.30 eV and 1.23 eV, respectively. The SBH variation between the Al-pristine and N-pristine interface is owing to the material polarization along the c-axis, while a feasible reason of the striking difference when the vacancy is induced can be explained by the different charge transfer. In the case of N-terminated interface, a less significant charge transferring from Au slab to AlN slab is found. And the tendency of the higher Schottky barrier height for the cation-terminated interface has been observed experimentally in GaN polar surface [40]. Besides, the SBHs are 2.41 eV and 2.21 eV for Al-V_{Al} and N-V_N interface, respectively. This higher SBH value for the N-V_N system could be further explained by the fact that less charge transfers from Au to AlN in comparison with N-pristine system, leading to the upward movement of Fermi level and the increase of the *p*-type SBH. Moreover, for Al-V_{Al} heterojunction, more electron losses in AlN raises the AlN band edge with respect to Au and hence gives rise to the SBH. The experimental value in Table 3 is taken as reference and the quantitative difference may exist in the defectives. The experimental samples may possess border or bulk defectives as well as some other inevitable impurities (e.g., O and C). However, the wide-spread values of the SBH are still within the numerical range reported before [17,44–46]. Based on the analyses above, the SBH of Au/AlN heterojunction shows unambiguous dependence on the interfacial condition as the vacant defect can significantly impact the barrier height.

4. Conclusion

In conclusion, the SBHs of Au/AlN heterojunction with different interfacial configurations are studied in detail. In the most stable configuration, the interfacial Au atoms locate on top of the surface atoms for the N-terminated interface, while the Au atoms favor the hollow site for Al-terminated interface. After being introduced the interfacial aluminum or nitride vacancy sites, the structures show smaller binding energies and larger interlayer distances. The Mulliken bond population reveals mixing of covalent and ionic bonding, but the Al-terminated interface shows dominance of ionic bonding characteristic and the N-terminated interface shows dominance of covalent bonding feature. The layer resolved DOS indicates an apparent feature of MIGS behavior, with the surface states almost disappearing on the third layer for all systems. Stronger Fermi level pining could be found in the interface with vacancy than pristine structure. The larger *p*-type SBHs are observed for the defective interface and this may result from the different charge transfer in comparison with the pristine models. It must be emphasized that the detailed atomic geometry at the interface would impact the SBH to a considerable degree. The calculated SBHs are in good correspondence with the available experimental and theoretical results.

Acknowledgements

This work was supported by the National Natural Science Foundation of China (Grant No. 61974094), the Science & Technology Bureau of Shenzhen (Grant No. 20160520174438578), and an MOE tier 1 grant R-144-000-402-114.

Declaration of competing interest

The authors declared that there is no conflict of interest.

References

[1] S. Strite, GaN, AlN, and InN: a review, J. Vac. Sci. Technol. B 10 (1992) 1237.
[2] J.Y. Tsao, S. Chowdhury, M.A. Hollis, D. Jena, N.M. Johnson, K.A. Jones, R.J. Kaplar, S. Rajan, C.G. Van de Walle, E. Bellotti, C.L. Chua, R. Collazo, M.E. Coltrin, J.A. Cooper, K.R. Evans, S. Graham, T.A. Grotjohn, E.R. Heller, M. Higashiwaki, M.S. Islam, P.W. Juodawlkis, M.A. Khan, A.D. Koehler, J.H. Leach, U.K. Mishra, R.J. Nemanich, R.C.N. Pilawa-Podgurski, J.B. Shealy, Z. Sitar, M.J. Tadjer, A.F. Witulski, M. Wraback, J.A. Simmons, Ultrawide-bandgap semiconductors: research opportunities and challenges, Adv. Electron. Mater. 4 (2018) 1600501.
[3] A. Khan, K. Balakrishnan, T. Katona, Ultraviolet light-emitting diodes based on group three nitrides, Nat. Photon. 2 (2008) 77–84.
[4] C. Hartmann, J. Wollweber, S. Sintonen, A. Dittmar, L. Kirste, S. Kollowa, K. Irmscher, M. Bickermann, Preparation of deep UV transparent AlN substrates with high structural perfection for optoelectronic devices, CrystEngComm 18 (2016) 3488–3497.
[5] H. Fu, I. Baranowski, X. Huang, H. Chen, Z. Lu, J. Montes, X. Zhang, Y. Zhao,

Demonstration of AlN schottky barrier diodes with blocking voltage over 1 kV, IEEE Electron. Device Lett. 38 (2017) 1286–1289.
[6] Q. Zhou, H. Wu, H. Li, X. Tang, Z. Qin, D. Dong, Y. Lin, C. Lu, R. Qiu, R. Zheng, J. Wang, B. Li, Barrier inhomogeneity of schottky diode on nonpolar AlN grown by physical vapor transport, IEEE J. Electron Devices Soc. 7 (2019) 662–667.
[7] O. Kovalenkov, V. Soukhoveev, V. Ivantsov, A. Usikov, V. Dmitriev, Thick AlN layers grown by HVPE, J. Cryst. Growth 281 (2005) 87–92.
[8] M. Takeuchi, H. Shimizu, R. Kajitani, K. Kawasaki, T. Kinoshita, K. Takada, H. Murakami, Y. Kumagai, A. Koukitu, T. Koyama, S.F. Chichibu, Y. Aoyagi, Al- and N-polar AlN layers grown on c-plane sapphire substrates by modified flow-modulation MOCVD, J. Cryst. Growth 305 (2007) 360–365.
[9] V.G. Mansurov, A.Y. Nikitin, Y.G. Galitsyn, S.N. Svitasheva, K.S. Zhuravlev, Z. Osvath, L. Dobos, Z.E. Horvath, B. Pecz, AlN growth on sapphire substrate by ammonia MBE, J. Cryst. Growth 300 (2007) 145–150.
[10] W.H. Chen, Z.Y. Qin, X.Y. Tian, X.H. Zhong, Z.H. Sun, B.K. Li, R.S. Zheng, Y. Guo, H.L. Wu, The physical vapor transport method for bulk AlN crystal growth, Molecules 24 (2019) 1562.
[11] T.Y. Chemekova, O.V. Avdeev, I.S. Barash, E.N. Mokhov, S.S. Nagalyuk, A.D. Roenkov, A.S. Segal, Y.N. Makarov, M.G. Ramm, S. Davis, G. Huminic, H. Helava, Sublimation growth of 2 inch diameter bulk AlN crystals, Phys. Status Solidi (c) 5 (2008) 1612–1614.
[12] S.B. Schujman, L.J. Schowalter, R.T. Bondokov, K.E. Morgan, W. Liu, J.A. Smart, T. Bettles, Structural and surface characterization of large diameter, crystalline AlN substrates for device fabrication, J. Cryst. Growth 310 (2008) 887–890.
[13] R. González-Hernández, A. González-Garcia, W. López-Perez, Density functional theory study of the adsorption and incorporation of Sc and Y on the AlN(0001) surface, J. Cryst. Growth 443 (2016) 1–7.
[14] A. González-García, W. López-Pérez, R. González-Hernández, Ab initio calculations of magnetic properties of Ag-doped GaN, Comp. Mater. Sci. 55 (2012) 171–174.
[15] L.J. Brillson, The structure and properties of metal-semiconductor interfaces, Sur. Sci. Rep. 2 (1982) 123–326.
[16] Z. Gao, Z. Zhou, D. Tomanek, Degenerately doped transition metal dichalcogenides as ohmic homojunction contacts to transition metal dichalcogenide semiconductors, ACS Nano 13 (2019) 5103–5111.
[17] P. Reddy, I. Bryan, Z. Bryan, J. Tweedie, R. Kirste, R. Collazo, Z. Sitar, Schottky contact formation on polar and non-polar AlN, J. Appl. Phys. 116 (2014) 194503.
[18] A. Slepko, J. Ramdani, A.A. Demkov, Schottky barrier at the AlN/metal junction, J. Appl. Phys. 113 (2011) 013707.
[19] B.L. Ward, J.D. Hartman, E.H. Hurt, K.M. Tracy, R.F. Davis, R.J. Nemanich, Schottky barrier height and electron affinity of titanium on AlN, J. Vac. Sci. Technol. B 18 (2000) 2082.
[20] S.J. Clark, M.D. Segall, C.J. Pickard, P.J. Hasnip, M.I.J. Probert, K. Resson, First principles methods using castep, Z. Kristallogr. 220 (2005) 567–570.
[21] J.P. Perdew, K. Burke, M. Ernzerhof, Generalized gradient approximation made simple, Phys. Rev. Lett. 77 (1996) 3865–3868.
[22] J. Heyd, G.E. Scuseria, M. Ernzerhof, Erratum: "Hybrid functionals based on a screened coulomb potential" [J. Chem. Phys. 118, 8207 (2003)], J. Chem. Phys. 124 (2006) 219906.
[23] M. Feneberg, R.A.R. Leute, B. Neuschl, K. Thonke, M. Bickermann, High-excitation and high-resolution photoluminescence spectra of bulk AlN, Phys. Rev. B 82 (2010) 075208.
[24] S. Tojo, R. Yamamoto, R. Tanaka, Q.T. Thieu, R. Togashi, T. Nagashima, T. Kinoshita, R. Dalmau, R. Schlesser, H. Murakami, R. Collazo, A. Koukitu, B. Monemar, Z. Sitar, Y. Kumagai, Influence of high-temperature processing on the surface properties of bulk AlN substrates, J. Cryst. Growth 446 (2016) 33–38.
[25] D. Ehrentraut, Z. Sitar, Advances in bulk crystal growth of AlN and GaN, MRS Bull. 34 (2011) 259–265.
[26] M.S. Miao, A. Janotti, C.G. Van de Walle, Reconstructions and origin of surface states on AlN polar and nonpolar surfaces, Phys. Rev. B 80 (2009) 155319.
[27] Y. Guo, D. Liu, J. Robertson, 3D Behavior of schottky barriers of 2D transition-metal dichalcogenides, ACS Appl. Mater. Interfaces 7 (2015) 25709–25715.
[28] J. Chen, Z. Zhang, Y. Guo, J. Robertson, Schottky barrier height at metal/ZnO interface: a first-principles study, Microelectron. Eng. 216 (2019) 111056.
[29] Z. Zhang, Q. Qian, B. Li, K.J. Chen, Interface engineering of monolayer MoS_2/GaN hybrid heterostructure: modified band alignment for photocatalytic water splitting application by nitridation treatment, ACS Appl. Mater. Interfaces 10 (2018) 17419–17426.
[30] J. Hu, W. Duan, H. He, H. Lv, C. Huang, X. Ma, A promising strategy to tune the Schottky barrier of a $MoS_{2(1-x)}Se_{2x}$/graphene heterostructure by asymmetric Se doping, J. Mater. Chem. C 7 (2019) 7798–7805.
[31] Q. Fang, Y. Huang, Y. Miao, K. Xu, Y. Li, F. Ma, Interfacial defect engineering on electronic states of two-dimensional AlN/MoS_2 heterostructure, J. Mater. Chem. C 121 (2017) 6605–6613.
[32] N.R. D'Amico, G. Cantele, C.A. Perroni, D. Ninno, Electronic properties and Schottky barriers at ZnO-metal interfaces from first principles, J. Phys.: Condens. Matter 27 (2015) 015006.
[33] J. He, E. Wu, H. Wang, R. Liu, Y. Tian, Ionicities of boron-boron bonds in B_{12} icosahedra, Phys. Rev. Lett. 94 (2005) 015504.
[34] D. Duan, X. Huang, F. Tian, Y. Liu, D. Li, H. Yu, B. Liu, W. Tian, T. Cui, Predicted formation of H_3^+ in solid halogen poly hydrides at high pressures, J. Phys. Chem. A 119 (2015) 11059–11065.
[35] J. Robertson, Band offsets of wide-band-gap oxides and implications for future electronic devices, J. Vac. Sci. Technol. B 18 (2000) 1785–1791.
[36] J. Robertson, Band offsets, Schottky barrier heights, and their effects on electronic devices, J. Vac. Sci. Technol. A 31 (2013) 050821.
[37] J. Ning, R. Li, X. Shen, Z. Qian, S. Hou, A.R. Rocha, S. Sanvito, First-principles calculation on the zero-bias conductance of a gold/1,4-diaminobenzene/gold molecular junction, Nanotechnology 18 (2007) 345203.
[38] Y. Liu, Z. Gao, Y. Tan, F. Chen, Enhancement of out-of-plane charge transport in a vertically stacked two-dimensional heterostructure using point defects, ACS Nano 12 (2018) 10529–10536.
[39] R.T. Tung, The physics and chemistry of the Schottky barrier height, Appl. Phys. Rev. 1 (2014) 011304.
[40] U. Karrer, O. Ambacher, M. Stutzmann, Influence of crystal polarity on the properties of Pt/GaN Schottky diodes, Appl. Phys. Lett. 77 (2000) 2012–2014.
[41] L.J. Brillson, Y. Dong, F. Tuomisto, B.G. Svensson, A.Y. Kuznetsov, Interplay of native point defects with ZnO Schottky barriers and doping, J. Vac. Sci. Technol. B 30 (2011) 050801.
[42] M.W. Allen, S.M. Durbin, Influence of oxygen vacancies on Schottky contacts to ZnO, Appl. Phys. Lett. 92 (2008) 122110.
[43] Z. Zhang, Y. Guo, J. Robertson, Chemical bonding and band alignment at X_2O_3/GaN (X = Al, Sc) interfaces, Appl. Phys. Lett. 114 (2019) 161601.
[44] R. Collazo, R. Schlesser, A. Roskowski, R.F. Davis, Z. Sitar, Hot electron transport in AlN, J. Appl. Phys. 88 (2000) 5865–5869.
[45] M. Morita, K. Tsubouchi, N. Mikoshiba, S. Yokoyama, Interface barrier heights in metal-aluminum nitride-silicon structure by internal photoemission, J. Appl. Phys. 53 (1982) 3694–3697.
[46] P. Reddy, I. Bryan, Z. Bryan, W. Guo, L. Hussey, R. Collazo, Z. Sitar, The effect of polarity and surface states on the Fermi level at III-nitride surfaces, J. Appl. Phys. 116 (2014) 123701.